Shear-induced metastable states of end-grafted polystyrene

Leslie A. Sasa, Eric J. Yearley, Michael S. Jablin, Robert D. Gilbertson, Adrienne S. Lavine, Jaroslaw Majewski, and Rex P. Hjelm

Phys. Rev. E **84**, 021803 — Published 5 August 2011

DOI: 10.1103/PhysRevE.84.021803

Shear-Induced Metastable States of End-Grafted Polystyrene

Leslie A. Sasa,*,+ Eric J. Yearley,* Michael S. Jablin,* Robert D. Gilbertson,* Adrienne S. Lavine,+ Jaroslaw Majewski,* & Rex P. Hjelm*,$

**Los Alamos Neutron Scattering Center, Los Alamos National Laboratory, Los Alamos, NM 87545, USA*

+Mechanical and Aerospace Engineering Department, University of California, Los Angeles, Los Angeles, CA 90095, USA

$Author to whom correspondence should be addressed; Electronic mail: hjelm@lanl.gov

The *in-situ* molecular scale response of end-grafted polystyrene to shear against a deuterated polystyrene melt was investigated with neutron reflectometry. The derived grafted polystyrene density profiles showed that the grafted polystyrene was retained on the quartz wafer during the measurements. The profiles suggested that the end-grafted polystyrene response to shear results in a series of metastable states, rather than equilibrium states assumed in the current theory. Except for some possible extension and/or contraction of the grafted polystyrene with shear, there was no obvious correlation between the grafted polymer structure and the shear thinning behavior observed in these samples.

Neutron reflectometry, neutron rheometer, grafted polymers, polymer melt, viscoelasticity

I. Introduction

The structural conformations of end-grafted polymers, attached at one end to a surface or interface, have been an area of interest in theoretical and experimental studies of non-linear viscoelastic properties. Shear thinning is one example of a non-linear viscoelastic response exhibited by polymeric materials, including end-grafted polymers, in which viscosity decreases with increasing shear rate.

Three plausible theories have been posited to explain shear thinning in grafted polymers and polymer composites. For example, such effects may be related to slip-shear, or wall-slip [1,2], which has been proposed to result from the disentanglement of surface-bound polymer from the bulk [3]. Besides disentanglement of surface-bound polymer from the bulk [3], other possibilities include changes in the local conformations of the polymer in the bulk and the tube

produced by the mean field interactions of its neighbors [4]; exchange of polymer at an interface [5]; or a combination of the aforementioned phenomena.

A number of theoretical and experimental studies have been undertaken to understand end-grafted polymer static structural conformations in contact with a solvent. Scaling laws [3,6] as well as analytical and mean field/self-consistent field approximation models [7] have been proposed to describe the molecular morphologies of grafted polymers. It is now widely accepted [8] that grafted polymers against a good solvent [9,10] exhibit a parabolic-type density profile with a Gaussian-like tail region.

Theories and experiments to determine the nature of grafted polymers under dynamic conditions, such as solvent flow, were devised and conducted shortly after a consensus concerning grafted polymers in static conditions was reached. In order to provide insight into this problem, neutron reflectivity measurements using a shear cell developed by Baker *et al*. [11] were implemented by several research groups [12]. These measurements led to the conclusion that the grafted polymers tilted and elongated in the direction of the solvent flow, but their overall height remained unaltered, in agreement with the models developed by Alexander and Rabin [13] and Miao *et al.* [14].

For the case of a grafted polymer in contact with a polymer melt, de Gennes *et al.* [15] hypothesized that the grafted polymers entangled with the melt at rest, then tilted and extended at low and intermediate shear rates. According to this model, at a higher, critical flow velocity, the grafted polymer disentangled completely from the melt.

Sternstein [5] proposed a competing explanation for the behavior of the grafted polymer under shear, in which the grafted chains that are entangled with the melt, release at a critical

shear rate and are replaced by chains from the melt. These grafted chains may totally desorb at sufficiently high shear rates, leaving a bare surface.

Presently, direct experimental data on the molecular response of an end-grafted polymer and polymer melt interface under shear is lacking. The objective of this study was to measure the behavior of an end-grafted polystyrene (PS) layer entangled with a deuterated polystyrene (dPS) melt under flow probed with neutron reflectometry (NR) as a function of shear rate using a newly developed state-of-the-art neutron rheometer [16]. The purpose of these measurements was to assess the role of the interaction between the grafted PS and the dPS melt in shear thinning.

II. Experimental Details

Protonated PS with a molecular weight of 82 kDa and polydispersity index of 1.05, measured by gel permeation chromatography calibrated for PS, was end-grafted onto the surface of a quartz wafer. The grafting procedure was similar to that used by Sasa *et al*. [16] and Karim *et al*. [10]. The grafted PS was placed in contact with a dPS melt with a molecular weight of 34.1 kDa and a polydispersity index of 1.19.

The neutron reflectometry experiments were performed using the Surface Profile Analysis Reflectometer (SPEAR) at the Los Alamos Neutron Science Center. SPEAR uses time--of-flight methods to measure reflectivity (the ratio of reflected to incident neutrons, R) as a function of momentum transfer normal to the sample surface, $Q_z = (4\pi/\lambda)\sin\theta$ using a neutron wavelength range of 1.5—16 Å (θ is the incident angle and λ is the incident neutron wavelength). The reflectivity data are reported as $R(Q_z)\times Q_z^4$, in order to highlight deviations in

the reflectivity profile from its quickly decaying envelope described by Fresnel's Law: $R \propto Q_z^{-4}$ [17].

The interfacial region between the end-grafted PS in contact with the dPS melt was studied as a function of shear rate using the Los Alamos Neutron Science Center neutron rheometer in the cone and plate geometry (CAPLNR) [16]. This instrument allows concurrent NR and rheological measurements under high torque—max. ~200 Nm, high shear rate—max. ~800 s^{-1}, and high temperature—max. ~200 °C conditions to study the flow of highly viscous polymer melts [16]. The scattering from the end-grafted PS was first measured at room temperature in air, and then the grafted PS was placed in contact with the dPS melt at 190 °C [16]. NR measurements of the grafted PS in contact with the melt were done with the sample at rest and at shear rates between 1.4 and 30.2 s^{-1} at 190 ºC in an inert argon environment to prevent sample oxidation. After completing the shear experiments, the quartz wafer and dPS melt were manually separated, and the quartz wafer was measured again in air.

The NR data were analyzed using a model-dependent Parratt fitting algorithm and compared to a model NR profile created using the Abeles's matrix formalism [17]. A box model approach was used to fit the NR data, where the true scattering length density (SLD) distribution was modeled by a series of boxes each with an accompanying SLD (ρ), thickness, and roughness. An error function connects adjacent boxes and describes the interfacial roughness. Nine boxes were the minimum needed to adequately characterize the reflectivity data for the system and to simulate parabolic profiles as used in previous theoretical and experimental studies [1,10]. A large number of more complex models were attempted; however, within the context of the Parratt algorithm, no further physical insight was available since the resulting parameters were deemed to be unphysical. Thus, the model presented in this paper is believed to capture the

most important features of both the NR data and the system. For each NR profile, the model parameter space was searched first using genetic optimization, then a Levenberg-Marquadt nonlinear least-squares algorithm, and finally the fit was manually adjusted for physical relevance and χ^2 minimization [17]. The uncertainty in the fits was deemed to be ± 0.001, as fits outside this range did not satisfactorily represent the data.

For each model, the volume fraction, $\phi(z)$, of grafted polymer, at distance z from the plate surface, was calculated independently from the SLD distribution, $\rho(z)$, as,

$$\phi(z) = \frac{\rho(z) - \rho_{dPS}}{\rho_{PS} - \rho_{dPS}} \quad (1)$$

The total volume of grafted PS per unit area was calculated with the following,

$$v_A = \int_{z_1}^{z_2} \phi(z) dz, \quad (2)$$

where z_1 and z_2 define the boundaries of the grafted PS region. Both the average distance of the grafted PS distribution from the quartz plate, $\bar{z} = v_A^{-1} \int_{z_1}^{z_2} \phi(z) z dz$, and the square root of the second moment,

$$R_z = \left(v_A^{-1} \int_{z_1}^{z_2} \varphi(z) z^2 dz \right)^{1/2}, \quad (3)$$

were calculated for each volume fraction distribution.

III. Results and Discussion

The end-grafted PS was first measured in air, then against a dPS melt at zero shear, and finally under a series of shear rates (summarized in Table I). Examples of the reflectivity profiles of the interface at rest (when first put in contact with the dPS melt) and under low shear (at a rate of 1.4 s^{-1}) are shown in FIG. 1. In FIG. 1 and FIG. 2a, the NR data are plotted as

colored markers while the corresponding model fits are plotted as black lines in FIG. 2a. Examples of the volume fraction profiles, $\phi(z)$, (EQ. 1) derived from the models are presented in FIG. 3.

Modeling of the NR data from the dry grafted PS in air resulted in a constant SLD profile (FIG. 3) near the surface of the quartz plate. At approximately z = 50 Å, the SLD profile abruptly decreased to zero. This implies that the grafted PS had a thickness (h) of ~50 Å and exhibited a more step-like density profile with a sharp boundary at the PS-air interface. Assuming that the grafted PS in air possesses a density of ~1.05 g/cm^3, the chain density per unit area and ν_A of the bound chain in this case are $3.9*10^{-4}$ Å^{-2} and 50 Å, respectively. Since ν_A and h are both equal to 50 Å when $\phi(z) = 1$ for $0 \leq z \leq h$, this demonstrates that the model fit for the dry grafted PS in air is physically reasonable.

When placed in contact with the dPS melt, the model fit suggests that the grafted PS extended ~500 Å into the melt (FIG. 3), which is physically consistent with a swollen grafted PS layer. An 82 kDa PS chain has an ideal linear chain radius of gyration (Rg) and a contour length of ~78 Å and ~2010 Å, respectively. Comparison of the theoretical values and the actual thickness (500 Å), derived from the experimental data, might be taken as an indication that the chain is extended more than what is expected for an ideally swollen grafted PS layer, as was suggested in a previous study where the grafted polymer was swollen with toluene [10]. However, when a comparison between the R_z values of the grafted polymer in this study (EQ. 3 & Table I) and the values expected for an ideal-swollen grafted PS (~125 Å, determined by the parallel axis theorem from the ideal chain Rg) is made, it is observed that the extension of the grafted PS into the melt was not significantly different from the ideal swollen case. Accordingly, because the distance between chain anchor points, D, was 57 Å, the chains must

overlap, since the average boundary diameter for an ideal chain is approximately 200 Å. The dimensionless grafting density of the grafted PS was $\sigma = a/D = 0.024$, where a is the statistical segment length, approximately the same value observed in a previous study [10].

Measurement of the dPS melt molecular weight by gel permeation chromatography before and after the shear measurements shows that there was little change over the course of the experiments (molecular weight of 34.1 kDa before vs. 32.2 kDa after and polydispersity index of 1.19 before vs. 1.29 after), demonstrating that there was little to no degradation of the dPS melt due to oxidation or other factors, that might otherwise have significantly affected the results. A similar determination for the grafted PS could not be made since it was not possible to recover the grafted PS after the measurements (as described in further detail later in the manuscript). However, throughout the entire experiment, the amount of end-grafted PS was conserved: The standard deviation of the integrated volume fraction profile, ν_A, (EQ. 2) in FIG. 3, given in Table I, was no more than ±10% from the mean value (45 ± 4Å) over the course of the entire experiment. This observation implied that the grafted PS was not removed from the quartz plate through degradation, release and/or exchange into the dPS melt by the applied shear.

Table I. Summary of shear experiments on end-grafted PS against a dPS melt.

Experiment Order of Data Collection	Shear Rate (s^{-1})	Conformational State	Viscosity (Pa s)	ν_A (Å)	$\overline{z}$ (Å)	R_z (Å)
Grafted PS in air	-	-	-	50	25	29
1	0	0	-	46	82	120
2	1.4	1	116	45	83	122
3	0	1	-	45	83	122
4	5.0	2	53.3	41	73	109
5	0	3	-	40	79	132
6	5.0	2	64.4	41	73	109
7	0	4	-	51	110	185
8	10.1	1	47.1	45	83	122
9	0	1	-	45	83	122
10	15.1	2	52.7	41	73	109
11	20.2	2	48.8	41	73	109
12	10.1	2	61.8	41	73	109
13	30.2	2	45.9	41	73	109
14	0	5	-	41	73	112

While 14 NR data sets were collected during the course of the shear measurements, only 6 distinct end-grafted PS structural states were observed. The reflectivity profiles from each individual measurement within experimental error of each other were fit to the same model, and thus, interpreted to be in the same structural state. Some states, while distinct according to this criterion, were otherwise similar. An example of this can be observed in the comparison of state 0 (when the grafted PS was first put in contact with the dPS melt) with state 1 (when exposed to a low shear rate of 1.4 s^{-1}). Under shear, the NR profile of state 1 (FIG. 1) at higher Q_z shifted to smaller values, which led to a slightly smaller $\phi(z)$ for z less than 15 Å. At larger z, however, the $\phi(z)$ of states 0 and 1 are identical and the chain extension ($\overline{z}$) as well as R_z (Table I) were also nearly equivalent. When considering the overall chain extension, it is clear that the states fall into three classes. Using R_z (Table I) as a guide: States 0 and 1 show the same, almost ideal extension; states 2 and 5 exhibit grafted PS which is slightly contracted; while states 3 and 4

feature grafted PS that is more extended. However, there are several differences in the details of the chain conformations of the various states that are discussed below.

In the z = 5—25 Å region, the $\phi(z)$'s for all states feature an initial parabolic profile with the form, $\phi(z) = \phi_0\left(1 - \left(z/H\right)^2\right)$, where ϕ_0 is the maximum volume fraction near the anchor point and H is the grafted PS height. This kind of parabolic-type profile was observed in previous studies of grafted PS against a good solvent [10]. . However, the value of H extracted from the fit for all the states was approximately 41 Å, less than one twelfth of the observed value. Beyond this region, for z = 25—175 Å, the grafted PS volume fraction profiles for all states show a long tail that declines monotonically with z (FIG. 3). In this region, state 1 (observed under shear and at rest after shear) demonstrated a slightly greater extension than states 0, 2, 3 and 5 while state 4 (observed at rest after the 2nd shear rate of 5.0 s^{-1}) showed distinctively different behavior with less extension of the tail into the melt.

An interesting feature observed in all the states was the presence of a mushroom-like "blob" of grafted PS for z > 175 Å, in close proximity to the free ends of the grafted chains (FIG. 3). This aspect of the structural models was derived from the shoulder in the NR data at Q_z ~ 0.017 Å^{-1}. This shoulder becomes a more distinct peak in states 3 and 4 (FIG. 2a), resulting in the mushroom-like "blob" becoming more obvious in the density profiles (FIG. 3). Furthermore, a larger square root of the second moment, R_z, of the chain distribution relative to the quartz surface reflects the more extended nature of the grafted chains into the melt in states 3 and 4 (Table I). Thus, the mushroom-like conformation of the grafted polymer was enhanced with the sample at rest after the application of moderate shear (Table I: Experiments 5 and 7 corresponding to states 3 and 4, respectively). The mushroom-like region was largely, but not completely, disrupted by the subsequent application of shear.

Corollary to the observation of a "blob" of grafted chains extending into the melt was the observation of a depletion layer between the region of z where the $\phi(z)$ declines monotonically and the mushroom-like region. Questions naturally arise concerning this rather surprising observation. The depletion layer, and hence the "blob," cannot be attributed to a section of the grafted PS that was sheared from the quartz and released into the dPS melt, as the system readily reverts to a state observed earlier in the measurement sequence when the shear conditions were changed. Also, the volume per unit area of the grafted PS was conserved throughout the measurement sequence. Additionally, the depletion layer cannot be attributed to the entrapment of air. The SLD profile only deviates slightly from the SLD expected for dPS (FIG. 2b). If air was present in the system, the SLD would decline sharply towards zero. Thus, the observed $\phi(z)$ profile must be attributed to a depletion layer and a mushroom-like layer of increased grafted PS density distal to it.

The 6 conformational states of the grafted PS in this system were found to be dependent upon the shear history. This observation indicates the grafted polymer chains demonstrated metastability. In other words, the same states were not always reproducible under similar shearing conditions. While the initial shear rate did not lead to a substantial change in the $\phi(z)$ and hence, chain extension (FIG. 3), there were substantial alterations at the higher shear rates (Table I). However, during one particular experiment with a high shear rate, the grafted PS chain profile reverted back to its original state (Table I, Experiment 8). Additionally, the states with the larger mushroom-like regions were not observed again when the system was returned to rest after low or high shear rates.

The shoulder in the reflectivity data at Q ~ 0.017 $Å^{-1}$ required a minima in the model SLD profile at z ~ 400Å (FIG. 2b). This resulted in a corresponding peak at z ~ 400Å in the

volume fraction profile (FIG. 3), which was derived from the SLD values using EQ. 1. Properly fitting the shoulder at Q ~ 0.017 $Å^{-1}$ caused a second order peak around Q ~ 0.035 $Å^{-1}$. Although there may be a hint of this feature in the data, this feature is not as prominent in the NR data as it is in the case of the model. Both the position and intensity of the first order peaks (at Q ~ 0.017 $Å^{-1}$) have been accurately fitted. Thus, the position and magnitudes of the features in the SLD and corresponding volume fraction profiles correctly represent the data. The lack of a strong second order peak in the data indicates that there is uncertainty in the details of the shapes of these features. As a result, both the differences in the minima at ~ 250 Å and the differences in the volume fraction values for various states at high z values were not deemed to be significant.

These observations naturally lead to the question of the relationship of the structural response of the grafted PS under melt shear and its rheological properties (e.g. shear thinning) outlined in the introduction. Rheological measurements, shown in FIG. 4, indicated shear thinning behavior. These measurements were taken as the shear was increased in the CAPLNR both before the NR measurements as well as during the actual NR measurements. The viscosities measured with the CAPLNR (Table I) were in reasonable agreement with the literature [18]. In the region where the shear thinning is the greatest, state 2 predominates (Table I and FIG. 4). As mentioned before, state 2, while showing similar chain profiles in the parabolic domain to states 0, 1 and 5, showed a slight contraction of the grafted chains from the melt (R_z in Table I). The comparison of states 0, 2 and 5 with state 1 (the latter of which is more extended into the melt), might indicate an effect of this conformation on measured viscosity. However, the correlation is less obvious when considering that the same state 1 was observed at higher shear and lower viscosity later in the measurement sequence. Thus, there are no apparent

strict correlations between the shear thinning behavior and the various grafted polymer structural states.

After completing the shear experiments, the quartz wafer and dPS melt were manually separated in order to re-measure the NR profile of remaining PS in air. However, the subsequent NR measurement from the quartz plate showed that there was very little PS left on the quartz as a result of this manual separation. This highlights the importance of measuring the polymer response to shear *in situ*; since it is likely that the forces between the grafted PS and the entangled dPS melt are sufficiently high to detach the grafted PS from the quartz when the cone and plate are separated.

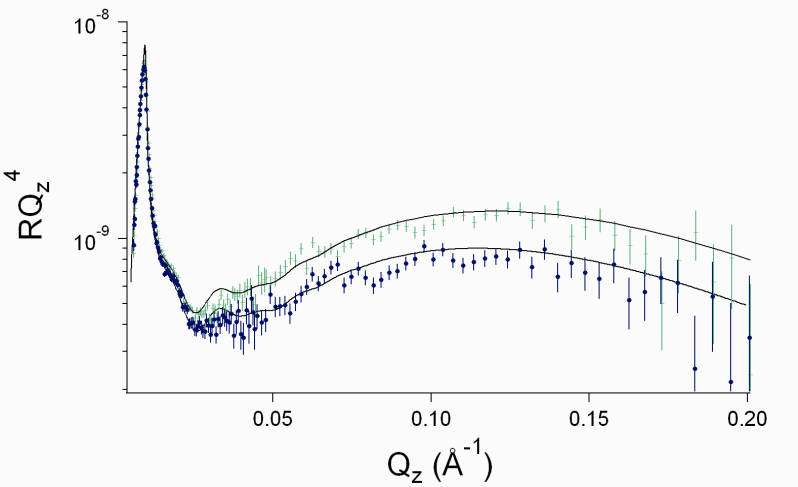

FIG. 1. (Color Online) (a) NR profiles of grafted PS against a dPS melt both at rest in state 0 (green crosses) and sheared at a rate of 1.4 s^{-1} in state 1 (blue circles). The NR data sets are plotted using colored markers and error bars indicating one standard deviation. The fits of the data are shown by the solid black lines.

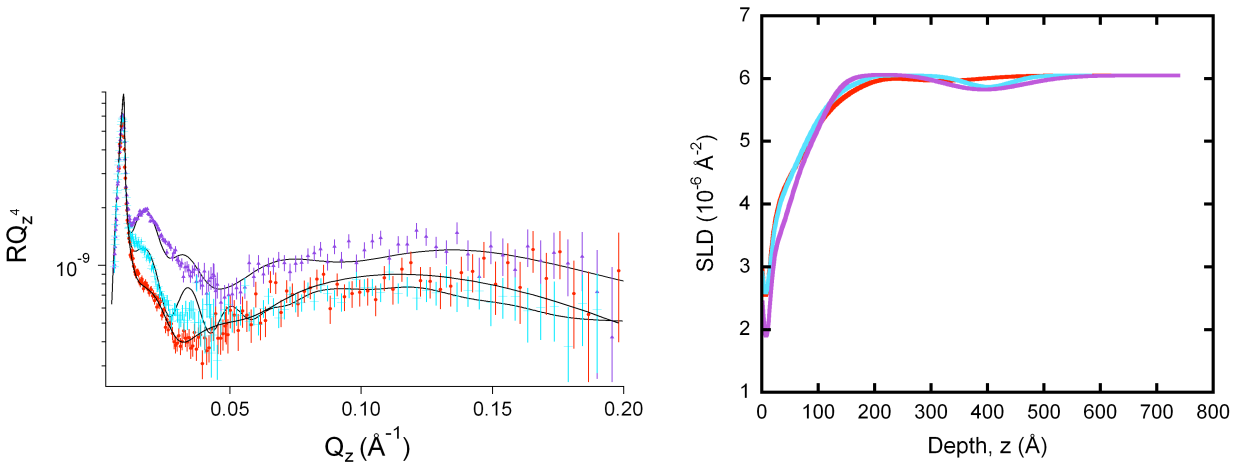

(a) (b)

FIG. 2. (Color) (a) NR profiles of the PS-dPS system in state 2 (red circles), state 3 (turquoise crosses) and state 4 (purple triangles). The NR data sets are plotted using colored markers and error bars indicating one standard deviation. The fits of the data are shown by the solid black lines. (b) The corresponding SLD profiles of state 2 (red), state 3 (turquoise) and state 4 (purple).

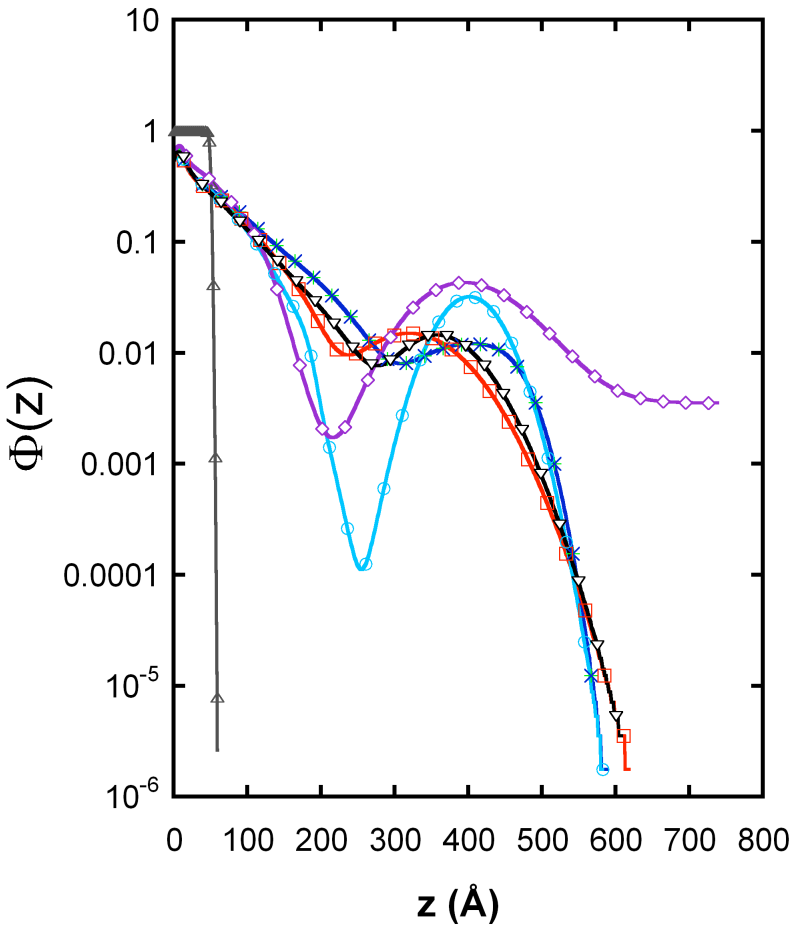

FIG. 3. (Color) Superimposed log-linear volume fraction profiles of end-grafted PS as a function of depth, *z*, from the quartz substrate. End-grafted PS in air (grey triangles); state 0: initial, no shear state, which follows the same curve as state 1, except at very low z values; state 1 (blue x's): sheared at 1.4 s^{-1} as well as at other shear rates and at rest as indicated in Table I, state 2 (red squares): sheared at various rates as shown in Table I; state 3 (turquoise circles): at rest after sheared at a low rate; and state 4 (purple diamonds): at rest after a moderate shear and state 5 (black inverted triangles): the final state at rest.

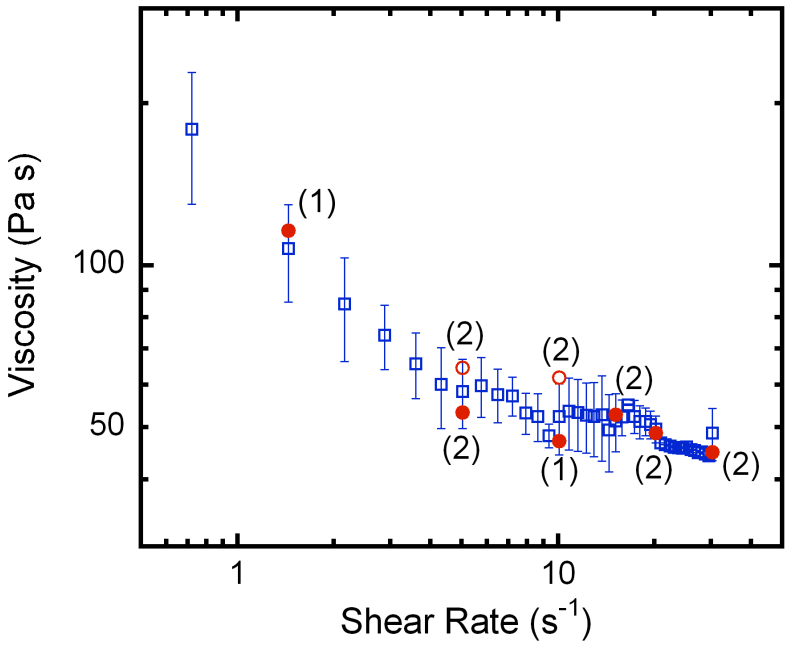

FIG. 4. (Color Online) Measured viscosity as a function of shear rate. Open blue squares show the average viscosity measured as the shear was increased in the CAPLNR before the NR measurements, where the error bars are the standard devations. Solid and open red circles show the steady state viscosity values measured during the actual NR measurements: the solid red circles were measurements taken as the shear rate was increased while the open red circles were measurements made as the shear rate was decreased. The numbers in the parentheses correspond to the states given in Table I and described in the text.

IV. Conclusion

The first *in situ* NR experiments in conjunction with rheological studies on the molecular responses of grafted PS in the interfacial region with a dPS melt under shear have been conducted using the CAPLNR. The results indicate that a grafted PS against a melt shows a volume fraction profile that is distinctly different from that observed against a good solvent. The results further show that the structural changes of the grafted PS under shear appear as metastable states. This indicates that the behavior of the grafted PS under shear may be dominated by non-equilibrium states that are not considered in current theory. Within the context of the observed shear thinning, polymer exchange of the grafted PS chains with the dPS

melt chains can be discounted as an explanation. Disentanglements of the grafted polymer from the melt during shear thinning, was not observed.

Acknowledgements

The authors thank Dr. Debra A. Wrobleski for the determination of the molecular weight distribution of the polystyrene. The authors would also like to thank Cynthia Welch for her invaluable assistance with this project. L. A. Sasa would like to gratefully acknowledge the National Physical Science Consortium and the Los Alamos National Laboratory Institute for Multiscale Materials Studies for their financial assistance. This work was supported by the use of the Lujan Neutron Scattering Center at LANSCE, which is funded by the Department of Energy's Office of Basic Energy Sciences. Los Alamos National Laboratory is operated by Los Alamos National Security LLC under DOE Contract DE-AC52-06NA25396.

References

[1] S. T. Milner, Science **251***,* 905 (1991).

[2] B. Zhao and W. J. Brittain, Prog. Polym. Sci. **25**, 677 (2000).

[3] P. G. de Gennes, Macromolecules **13**, 1069 (1980).

[4] J. Bent, L. R. Hutchings, R. W. Richards, T. Gough, R. Spares, P. D. Coates, I. Grillo, O. G. Harlen, D. J. Read, R. S. Graham, A. E. Likhtman, D. J. Groves, T. M. Nicholson, T. C. B. McLeish, Science **301**, 1691 (2003).

[5] S. S. Sternstein and A.-J. Zhu, Macromolecules **35**, 7262 (2002).

[6] S. Alexander, J. Phys. Paris **38**, 977 (1977). S. Alexander, J. Phys. Paris **38**, 983 (1977). P. G. de Gennes, J. Phys. Paris **37**, 1445 (1976). P. G. de Gennes, Adv. Colloid Interface Sci. **27**, 189 (1987).

[7] A. N. Semenov, Sov. Phys. JETP **61**, 733 (1985). C. Cosgrove, T. Heath, B. van Lent, F. Leermakers, J. Scheutjens Macromolecules **20**, 1692 (1987). A. M. Skvortsov, A. A.

Gorbunov, V. A. Pavlushkov, E. B. Zhulina, O. V. Borisov, V. A. Priamitsyn, Polym. Sci. USSR **30**, 1706 (1988). S. T. Milner, T. A. Witten, and M. E. Cates, Macromolecules **21**, 2610 (1988). S. T. Milner, T. A. Witten, and M. E. Cates, Macromolecules **22**, 853 (1989). S. T. Milner, Macromolecules **24**, 3704 (1991).

[8] P. Auroy, L. Auvray, and L. Léger, J. Phys.: Condens. Matter **2**, SA317 (1990). P. Auroy, L. Auvray, and L. Léger, Phys. Rev. Lett. **66**, 719 (1991). P. Auroy, L. Auvray, and L. Léger, Macromolecules **24**, 2523 (1991). S. H. Anastasiadis, T. P. Russell, S. K. Satija, C. F. Majkrzak, Phys. Rev. Lett. **62**, 1852 (1989). S. K. Satija, C. F. Majkrzak, T. P. Russell, S. K. Sinha, E. B. Sirota, G. J. Hughes, Macromolecules **23**, 3860 (1990). T. Cosgrove, T. G. Heath, J. S. Phipps, R. M. Richardson, Macromolecules **24**, 94 (1991). M. A. C. Stuart, T. Cosgrove and B. Vincent, Adv. Colloid Interface Sci. **24**, 143 (1986). T. Cosgrove, T. G. Heath, K. Ryan, T. L. Crowley, Macromolecules **20**, 2879 (1987).

[9] G. S. Smith, C. Toprakcioglu, S. M. Baker, J. B. Field, L. Dai, G. Hadziioannou, W. Hamilton, S. Wages, Il Nuovo Cimento **16**, 721 (1994). M. S. Kent, L. T. Lee, B. J. Factor, R. Rondelez, G. Smith, J. Phys. IV **3**, 49 (1993). J. B. Field, C. Toprakcioglu, R. C. Ball, H. B. Stanley, L. Dai, W. Barford, J. Penfold, G. Smith, W. Hamilton, Macromolecules **25**, 434 (1992). A. Karim, S. K. Satija, J. F. Douglas, J. F. Ankner, L. J. Fetters, Mat. Res. Soc. Symp. Proc. **304**, 149 (1994). D. L. Anastassopoulos, A. A. Vradis, C. Toprakcioglu, G. S. Smith, L. Dai, Macromolecules **31**, 9369 (1998). C. Marzolin, P. Auroy, M. Deruelle, J. P. Folkers, L. Leger, A. Menelle, A. **34**, 8694 (2001).

[10] A. Karim, S. K. Satija, J. F. Douglas, J. F. Ankner, and L. J. Fetters, Phys. Rev. Lett. **73**, 3407 (1994).

[11] S. M. Baker, G. Smith, R. Pynn, P. Butler, J. Hayter, W. Hamilton, L. Magid, Rev. Sci. Instrum. **65**, 412 (1994).

[12] D. Nguyen, C. J. Clarke, A. Eisenberg, M. H. Rafailovich, J. Sokolov, and G. S. Smith, J. Appl. Cryst. **30**, 680 (1997). D. L. Anastassopoulos, A. A. Vradis, C. Toprakcioglu, G. S. Smith, and L. Dai, Macromolecules **31**, 9369 (1998). S. M. Baker, A. Callahan, G. Smith, C. Toprakcioglu, A. Vradis, Physica B **241-243**, 1041 (1998). S. M. Baker, G. S. Smith, D. L. Anastassopoulos, A. A. Vradis, and D. G. Bucknall, Macromolecules **33**, 1120 (2000). R. Ivkov, P. D. Butler, S. K. Satija, and L. J. Fetters, Langmuir **17**, 2999 (2001).

[13] Y. Rabin and S. Alexander, Europhys. Lett. **13**, 49 (1990).

[14] L. Miao, H. Guo and M. J. Zuckermann, Macromolecules **29**, 2289 (1996).

[15] F. Brochard and P. G. de Gennes, Langmuir **8**, 3033 (1992); A. Ajdari, F. Brochard-Wyart, P. G. De Gennes, L. Leibler, J.-L. Viovy, and M. Rubenstein, Physica A **204**, 17 (1994). F. Brochard-Wyart, C. Gay, and P. G. de Gennes, Macromolecules **29**, 377 (1996).

[16] L. A. Sasa, E. J. Yearley, C. F. Welch, M. A. Taylor, R. D. Gilbertson, C. Hammeter, J. Majewski, and R. P. Hjelm, Rev. Sci. Instrum. **81**, 055102 (2010).

[17] A. Nelson, J. Appl. Crystallogr. **39**, 273 (2006).

[18] T. G. Fox and P. J. Flory, J. Polym. Sci. **14**, 315 (1954).